# Limb Broad-Band Imaging Spectrometer for the NPOESS Ozone Mapping and Profiler Suite (OMPS)

Michael G. Dittman, James Leitch, Michael Chrisp, Juan Rodriguez, Angela Sparks, Brian McComas,
Neal Zaun, Doug Frazier, Tom Dixon, Rob Philbrick, Debra Wasinger
Ball Aerospace & Technologies Corp.

## ABSTRACT

The Ozone Mapping and Profiler Suite (OMPS) is being developed for the United States National Polar-orbiting Operational Environmental Satellite System (NPOESS). We describe the optical design and predict the performance of the OMPS earth limb-imaging spectrometer. Limb-scattered solar radiation is measured at selected ultraviolet (UV), visible, and near infrared (NIR) wavelengths to determine ozone profile concentrations for the altitude range of 8 to 60 km. The sensor consists of a telescope with three separate crosstrack fields of view of the limb, a prism spectrometer covering 290 to 1050 nm, and a solar-diffuser calibration mechanism. The sensor provides 3 km vertical resolution profiles of atmospheric radiance with channel spectral resolutions (full-width at half-maximum, FWHM) ranging from 2.7 nm in the UV to 35 nm in the NIR and handles the demanding spectral and spatial dynamic range of the limb-scattered solar radiation with the required sensitivity for ozone retrievals.

Keywords: NPOESS, OMPS, Ozone, Limb Profile

## 1. INTRODUCTION

NPOESS, the National Polar-orbiting Operational Environmental Satellite System, will provide the U.S. with an enduring capability to measure, on a global basis, atmospheric, land, and ocean environmental parameters. The system will provide timely and accurate weather and environmental data to weather forecasters, military commanders, civilian leaders, and the scientific community. Ball Aerospace & Technologies Corp. has been contracted by the Department of Defense, Department of Commerce, and NASA to design and fabricate one of the sensor payloads slated to fly on NPOESS in 2008 – the Ozone Mapping and Profiler Suite (OMPS). OMPS will measure ozone levels in our atmosphere and how the ozone concentration varies with altitude. OMPS data will continue ozone fluctuation and trend measurements made by current sensors (TOMS, SBUV/2) and can be used to help determine if synthetic chemicals are affecting the Earth's climate and its habitability. The OMPS system consists of a modular 2-sensor design: a hyperspectral UV, visible, and near IR limb sensor and a wide-field hyperspectral UV nadir sensor. The preliminary design of the OMPS was presented at the Sapporo Quadrennial Ozone Symposium in July 2000[1]. This paper provides a general description of the design and performance of the limb sensor, with an emphasis on the optical design.

## 2. SCIENCE OVERVIEW

OMPS sensor and algorithm requirements were derived from NPOESS ozone environmental data record (EDR) performance requirements. The vertical cell size requirement threshold of 5 km drove the requirements for a separate limb sensor since the inherent vertical resolution of nadir ozone profiling is 8 to 12 km using backscattered solar radiation in the ultraviolet Hartley and Huggins absorption bands[2]. In addition, the vertical coverage EDR requirement (tropopause height to 60 km) could not be satisfied by the nadir profiling technique, which provides profile information independent of a priori assumptions in the 30-50 km range[2]. Remote sensing of limb-scattered solar radiation shares atmospheric radiative transfer physics as well as calibration techniques with the OMPS nadir sensor. Early on-orbit demonstration of limb scatter ozone profiling used measurements at 265 and 296 nm where single (Rayleigh) scattering is dominant, thereby restricting the technique to the mesosphere and upper stratosphere[3]. Aruga and Heath[4] extended the technique to longer ultraviolet wavelengths by considering multiple scattering, but this improved technique was still restricted to altitudes above ~25 km. Because of the great scientific interest in the behavior of ozone at and below the ozone peak, Herman et al.[5] showed that profiling could be extended down to 15 km using limb scatter measurements at 602 nm, the peak of the Chappuis absorption band. The combined visible-ultraviolet limb scatter technique was demonstrated by the Shuttle Ozone Limb Sounding Experiment / Limb Ozone Retrieval Experiment (SOLSE/LORE) flown on STS-87 in December 1997 [6,7].

Working with an algorithm team at Raytheon ITSS (formerly Hughes STX) led by Dr. Thomas Swissler and Dr. Jack Larsen, Ball developed the requirements for the OMPS limb sensor. The spectral range (290-1000 nm) and channel selection were determined by detailed analysis of several science and algorithm requirements, using the earlier work as a guide. A short wavelength limit of 290nm provides the required sensitivity at the upper end of the altitude range (60 km). Other channels in

the middle and near ultraviolet provide coverage down to 28 km. Several channels in the Chappuis band including 602 nm provide coverage between 28 km and the tropopause. Additional channels between 350 and 1000 nm provide characterization of the Rayleigh and aerosol scattering background. As with the OMPS nadir sensor and the TOMS and SBUV/2 instruments, the calibration stability essential for long-term monitoring of ozone is maintained on-orbit by periodic observations of the sun using a diffusing element to direct the solar irradiance into the telescope.

## 3. TECHNICAL CHALLENGES

The primary technical challenge in these science objectives is the large dynamic range inherent in the UV to NIR limb spectrum. The signal varies by 4 to 5 orders of magnitude across the measured spectral and vertical ranges. In addition, the precision requirements of the ozone profile retrieval demand that the sensor make measurements with high Signal to Noise Ratios (SNR), particularly in the visible spectral channels. The wide signal range requires the use of multiple gain ranges which are provided by different aperture areas and different integration times in the OMPS Limb Sensor.

The dynamic range of the limb scene and the stringent NPOESS reliability requirements, which make certain stray-light control techniques difficult, make designing for low stray light a high priority. This obviously includes minimizing the number of optical surfaces used. Finally, the mass and volume allocations for OMPS are challenging, requiring a compact and efficient system.

## 4. MECHANICAL DESIGN & ALLOCATIONS

The mechanical package of the limb sensor is shown in Figure 1. The technical driving requirements for the mechanical design of the OMPS limb sensor are mass, volume, and optical performance over a broad temperature range. The titanium structure has kept the mass of the sensor below 10 kilograms, 10 percent below the sensor's allocated mass. The mirror substrates are BK7 and produce a small but acceptable thermal focus shift in the limb optics. The sensor volume is 37.2 cm x 44.6 cm x 28.1 cm.

The configuration of the optics layout allows most of the optics assemblies to be accessed from outside the primary structure. Non-structural covers are installed over the optics assemblies, and labyrinth seals block external stray light. The packaging of the telescope and spectrometer optics uses stemmed, circumferencially-bonded optics. The spectrometer prism's mount thermally isolates the prism. The entire limb assembly is attached to the spacecraft using kinematic mounts.

## 5. OPTICAL DESIGN AND PERFORMANCE

The Limb Field of Regard (FOR) is shown in Figure 2. It consists of three individual Fields of View (FOV), each of which is 2.23° long separated cross-track by 4.253°. The center slit is aligned with the spacecraft ground track. From our orbital altitude of 833 km, the side slits view the limb at ±250km from the ground track.

The vertical Field of View (FOV) is driven by the system requirement to view 65 km of atmosphere at a limb tangent distance of 3365 km with margin for alignment and attitude control uncertainties, spacecraft orbital insertion and maintenance tolerances, and the earth's oblateness. Table 1 provides the FOV budget. Most of our analyses are performed assuming the configuration shown in Figure 2, with the 0 km limb being in the center of the FOVs. This is actually the extreme pointing case, providing the most stressing case for stray light effects since fully half of each slit is filled with relatively bright earth scene. The nominal pointing case will be when the 32 km altitude is centered in the FOV, which occurs when the optical axis is pointing 27.3° below the spacecraft platform and the spacecraft pointing, orbit and earth oblateness are all at their average values.

Overall sensor performance is described in Table 2. The three FOVs, defined by the three entrance slits to the spectrometer, are served by three separate telescopes. In addition, each telescope has two apertures of differing area (78.54mm$^2$ and 28.27mm$^2$). These two apertures produce two separate images in the spectrometer with a fixed intensity ratio. These bright and dim spectral images correspond to what we call the optical gain levels of the sensor. The large aperture produces the High Gain (HG) image and the small aperture produces the Low Gain (LG) image. The three telescopes with two apertures each therefore require a total of six entrance apertures into the sensor. The three telescopes feed a single prism-based spectrometer and charge-coupled device (CCD) focal plane. Figure 3 shows the layout of the large and small telescope apertures and the separate images on the detector resulting from the 6 apertures. Readout of the detector uses two different interleaved integration times to produce four gain levels for each slit image. They are (from highest to lowest gain): HG long, LG long, HG short, and LG short.
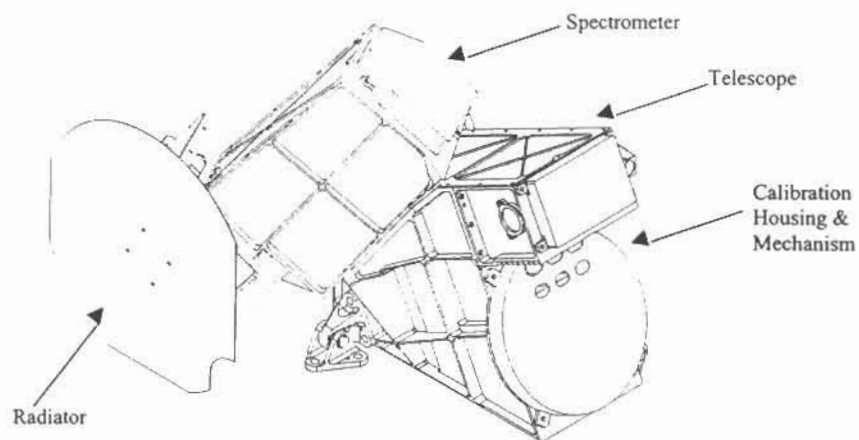
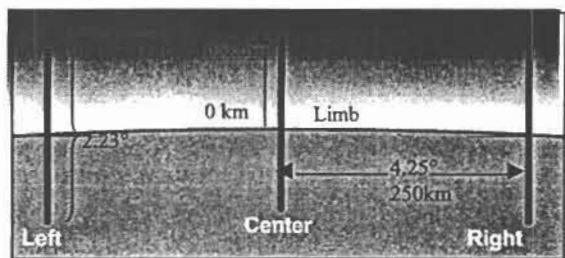Figure 1    Limb sensor mechanical layout. Dimensions are in centimeters.



Figure 2    Field of regard and entrance slit projections onto the Earth's limb

Table 1    Limb FOV Budget

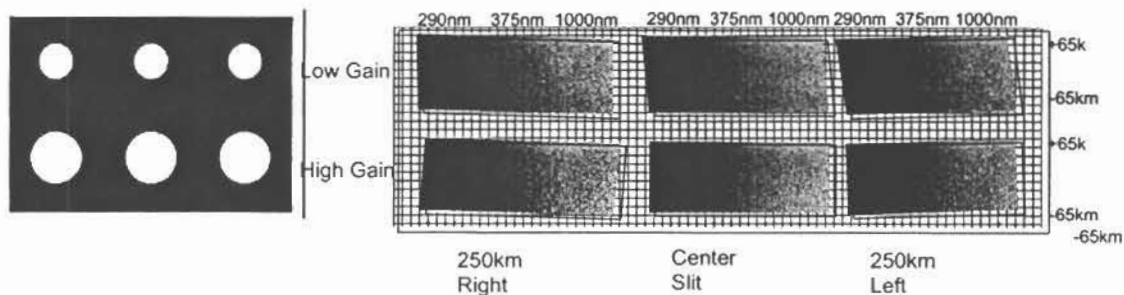| Parameter | Allocation (km) |
|---|---|
| Altitude Coverage | 65 |
| Alignment & Attitude | 15 |
| Earth Oblateness | 21 |
| Spacecraft Orbit | 30 |
| **Total** | **131** |

= 2.23°



Figure 3    Limb sensor entrance aperture and corresponding image layout on the CCD. The combination of the optical gain ratio with multiple integration times covers the large limb scene dynamic range.

TM2 (6)  Top-View of Telescope  TM1 (3)

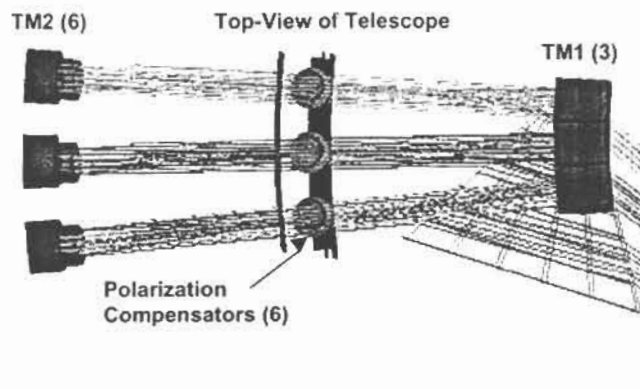Polarization
Compensators (6)

Figure 4    Top View of the afocal telescopes. Three telescopes combine into one spectrometer.

Each Limb Sensor telescope consists of an entrance aperture pair, a polarization compensator, a primary mirror (TM1) and an entrance slit (Figures 4 and 5). The first optical element in each path is a polarization compensator consisting of a single plate tilted to compensate for the polarization sensitivity resulting from the large angle of incidence on the prism faces and other polarization sensitive elements. The total linear polarization sensitivity of the instrument is reduced from 8% to 2% with these compensators. The Low Gain channels also have a neutral density filter located near the compensators. The TM1 mirrors are off-axis segments of a common paraboloidal parent mirror. The three TM1 segments are bonded together on a common substrate and mounting surface. Technically, the telescopes end at the slits, which are individually mounted and aligned. The performance of the telescopes up to the slits is described in the text accompanying Figure 6. As an opto-mechanical assembly, however, the collimating optics which follow the slits are included with the telescopes, making for an afocal assembly. These secondary mirrors (TM2) are additional off-axis paraboloid segments with the same radius of curvature as the TM1 mirrors. This makes each afocal telescope a pair of confocal parabolas. There are six separate TM2 mirrors, one for each telescope and aperture. A rotation applied to the LG TM2 mirrors separates the LG images on the detector from the HG images.

The system aperture stops (limiting apertures) follow the afocal telescopes (Figure 5). The apertures at the sensor entrance port are slightly oversized. The aperture stop plate completes the mechanical structure of the afocal telescope. The spectrometer consists of a fused silica prism and a two-mirror camera. The prism is made from a grade of fused silica that provides good UV transmission with little internal scatter. The spectrometer (prism and camera) can be aligned separately from the afocal telescope and then integrated. The image is focused onto the CCD after the subsystems are combined. All limb sensor mirrors are made from BK7 and are coated with Al overcoated with a protective layer of $SiO_2$.

Although the sensor can provide as many as 200 spectral channels for each detector image, only selected channels are sent to ground. The wavelength channels are constructed by combining up to 4 adjacent spectral pixels. The center wavelengths of the channels currently specified for downloading from the sensor are (in nm): 290, 293, 296, 299, 302, 310, 320, 347, 353, 400, 490, 500, 514, 525, 575, 602, 616, 632, 675, 750, and 1000. The spectral bandpass requirement increases with wavelength, getting wider as the ozone absorption spectral features become broader. The dispersion of the fused silica prism is well matched to the required spectral resolution.

The telescope design utilizes confocal pairs of off-axis parabolas. The three telescopes are identical, so the performance is presented here only for the center telescope. The slits provide a horizontal IFOV of 0.6mrad. The optical performance of the telescopes up to the slits is shown in Figure 6. The telescope is designed to give the best balance of image quality both at the slit and at the output of the afocal telescope, traded against mass and volume.
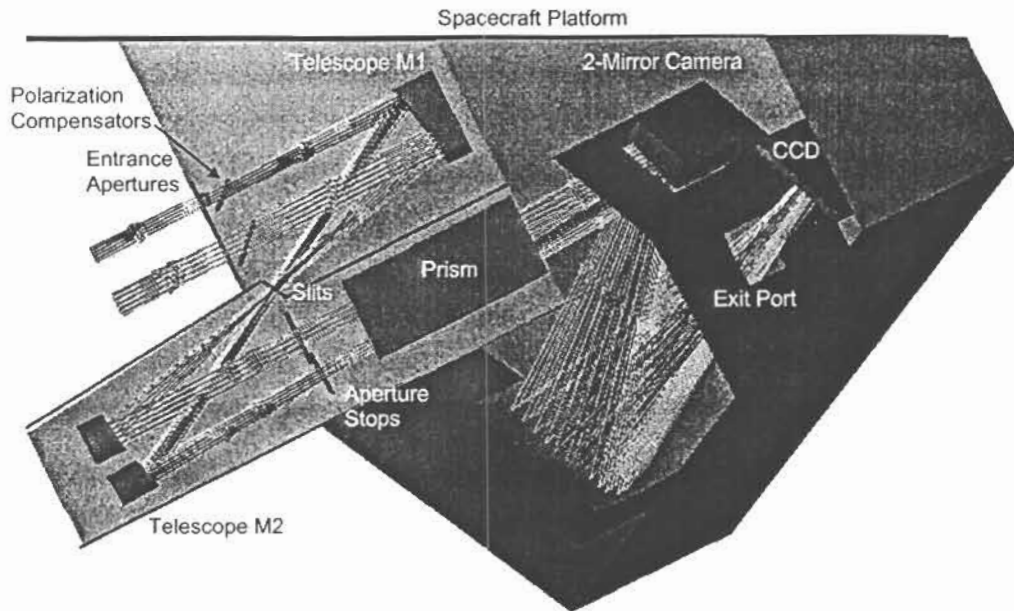
Spacecraft Platform

Figure 5  Limb sensor functional layout, side view shows compact design required by NPOESS allocations.

Table 2  Sensor Performance

| Parameter | Value (HG) | Value (LG) |
|---|---|---|
| Entrance Pupil Area | 78.54mm² | 28.27mm² |
| F-number at slits | F/9 | F/15 |
| Slit Width | 0.6mrad | |
| F-number at detector | F/6.9 | F/11.2 |
| System Effective Focal Length | 68.1 ± 0.7mm | 70.8 ± 1.6 mm |
| Transmittance (includes CCD QE) | 43.5% @ 290nm 3.2% @ 1020nm | 26.1% @ 290nm 1.9% @ 1020nm |
| Vertical FOV | 2.315° | |
| Vertical IFOV | 0.976 to 0.998km | |
| Vertical MTF @0.167cycles/km | ≥0.56 from 290 → 1050nm | |
| Horizontal sampling interval | 4.253° ± 0.085° | |
| Wavelength range | 288.5nm → 1020nm | |
| Bandpass (unbinned pixels) | FWHM ≤ 1.65nm @ 290nm | |
| Linear polarization sensitivity | < 2.0% | |
| Stray Light | < 4% in UV, < 10% in IR | |
| Pixel Size | 20µm spectral x 25µm spatial | |
| Used CCD area | 667 pixels spectral x 326 pixels spatial | |
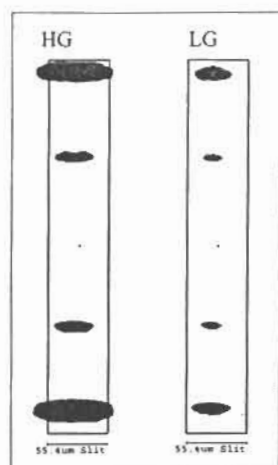
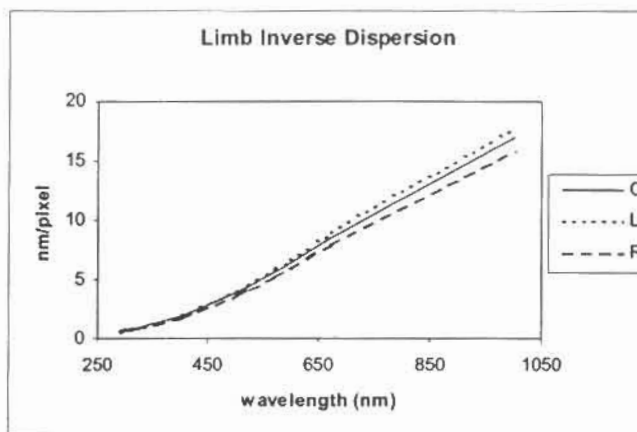Figure 6    Telescope Spot Diagrams



Figure 7    Spectral inverse dispersion in nm/pixel

The spectral performance of the limb sensor is mainly determined by the image of the slits at the detector. Figure 7 shows the inverse of the dispersion seen by the light through each of the three slits as a function of wavelength. Since shorter wavelengths see a greater dispersion in the prism, the spectral resolution of the sensor is likewise greatest at the short wavelengths. Figure 8 shows the geometric spot diagrams for the central slit (spectrometer only). A spectral channel is created from one or more spectral pixels through on-board binning. The spots are therefore shown relative to the spectral width of two pixels.

The spectral response function is found by convolving the optical point spread function (PSF) with the slit, the pixel and the detector diffusion and charge transfer efficiency (CTE) blur. The beginning-of-life (BOL) and end-of-life (EOL) spectral response functions are shown in Figure 9. The only difference between the two is the CCD CTE which is assumed perfect at BOL and degrades to the EOL condition gradually over time owing primarily to radiation damage. The spectral response varies from slit to slit, due entirely to the varying dispersion. The three slits are imaged through the prism at different angles, resulting in this dispersion difference. These curves do not include the effect of stray light or ghosting, which would not be seen at this scale at any rate.
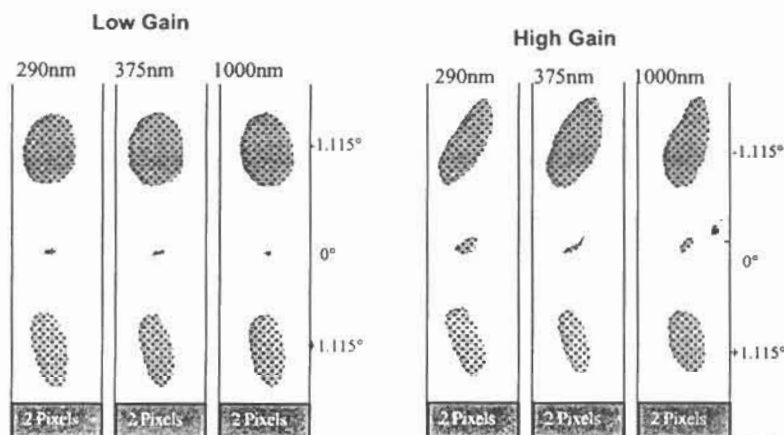


Figure 8    Spectrometer spot diagrams show image quality is well matched to resolution element (2 pixels minimum)
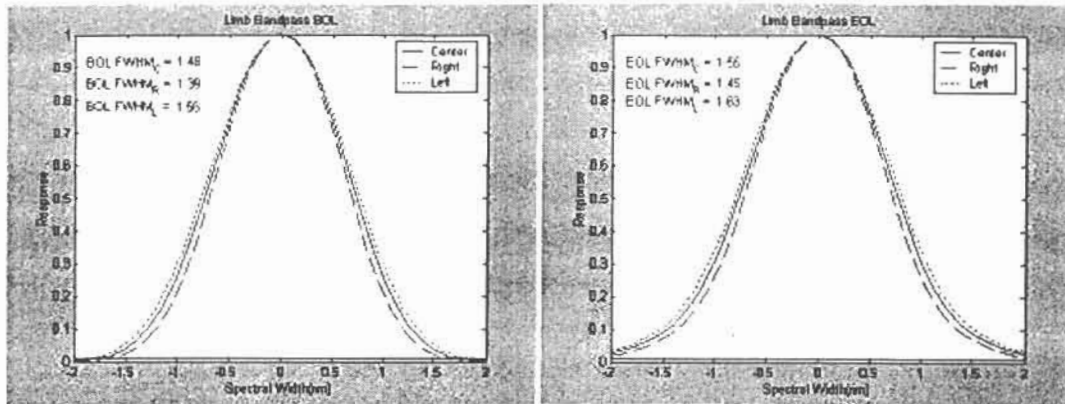
Figure 9    Spectral bandpass response at 290 nm at a field position of 0 degrees a) Beginning-of-Life (BOL), b) End-of-Life (EOL) shows small difference in FWHM for three slits (Center, Right, Left) and slight broadening in the response over the sensor lifetime.

The spatial performance of the limb sensor requires analysis of the entire optical train, from telescope to detector. The driving requirement is a vertical resolution of 3 km at the earth limb, where resolution is defined[8] as $1/(2f)$, where f is the spatial frequency corresponding to an MTF of 0.5. The focal length of the sensor is such that a single spatial pixel (20μm) corresponds approximately to 1 km at the limb. The optical performance of the ideal design (neglecting manufacturing and alignment tolerances and post-alignment motion) creates point source images of less than 1 pixel. These spots are shown for the center slit in Figure 10. The spatial response function, the convolution of the PSF with the pixel and the CCD diffusion and CTE blur, is shown in Figure 11. The spatial response includes the effects of ghost reflections off the CCD window and sensor stray light.
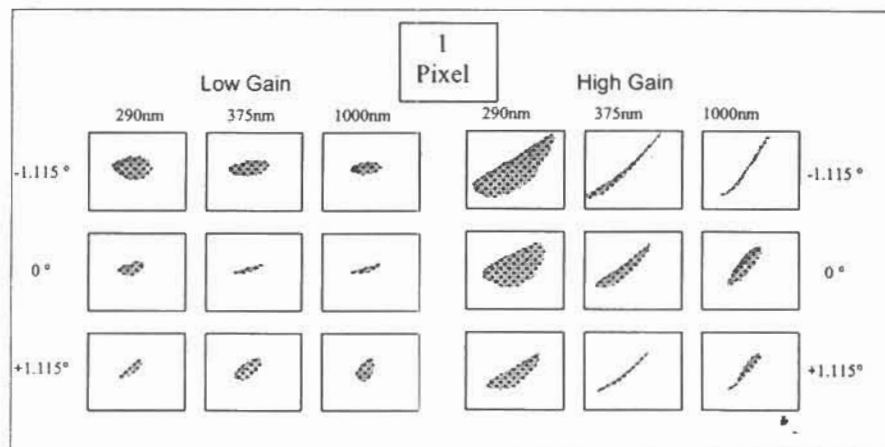


Figure 10    Spatial spot diagrams for the center slit. One pixel corresponds to ~1 km in the vertical dimension and 0.63 nm at 290 nm in the spectral dimension. Image quality is well matched to the pixel size.

Stray light is controlled through use of smooth surface finishes, tight contamination control, and spectral filtering at the focal plane.
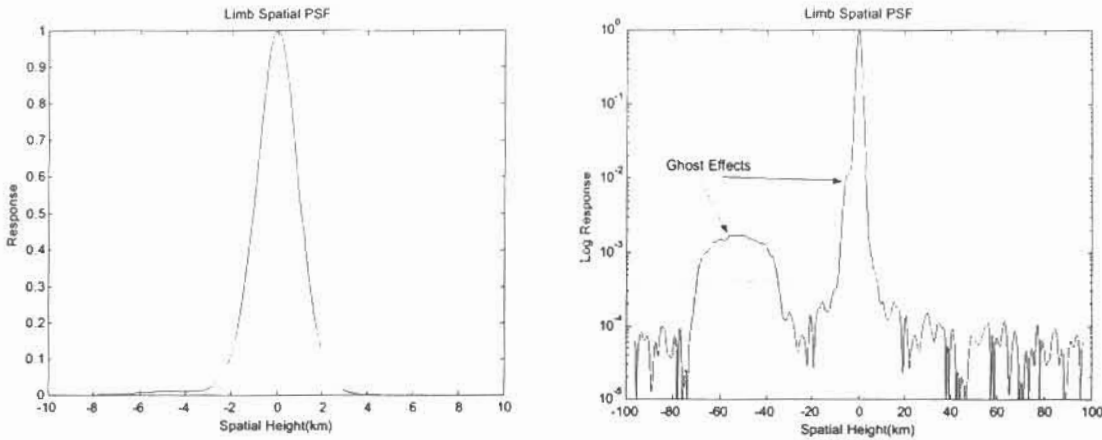
Figure 11    Vertical spatial PSF, plotted on a linear and on a logarithmic scale show relative effects of ghosting and scatter on the spatial resolution of the sensor.

Figure 12 shows the spectral efficiency of the limb sensor, with the various individual contributions split out. The mirror coating is optimized to produce a small degree of spectral flattening between the UV and visible wavelengths. Polarization is ignored for this analysis. The transmissions of the high and low-gain paths are identical except for the neutral density filters in the LG paths. The predicted transmission of the ND filter is 61% ± 2% from 200nm to 1500nm.
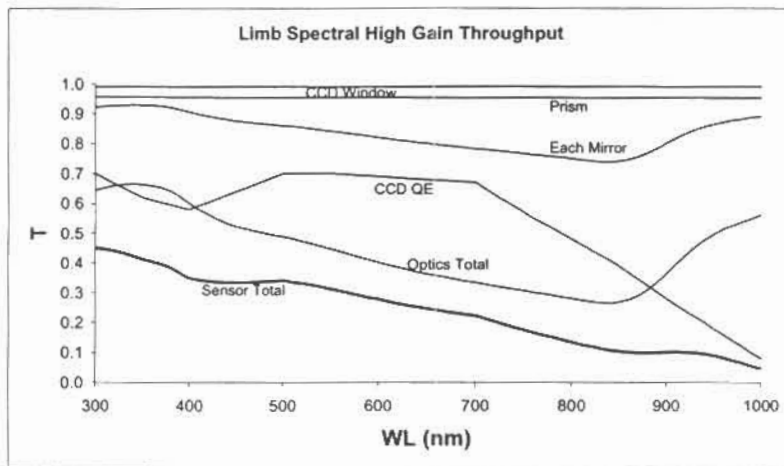


Figure 12    High-Gain Channel Spectral Efficiency or Transmission shows sensor is optimized for UV performance.

Stray light in the OMPS limb sensor varies with both altitude and wavelength. The main source of stray light is the scatter of light from different altitudes and wavelengths into the altitude and wavelength under consideration. This problem is greatest in the high altitude UV (290 nm), where the irradiance on the focal plane is over 3 orders of magnitude smaller than the irradiance on the focal plane at 500 nm, and in the NIR (700 to 1050 nm), where UV light from the adjacent slit spectral image overlaps the NIR bands. The worst-case stray light is 4.23% in the UV (290 nm, 60 km) and 10.25% in the IR (1000 nm, 45 km). The average stray light for visible wavelengths at altitudes between 0 km and 45 km is 0.42%. Figure 13 shows a typical mapping of stray light to wavelength and altitude in the scene.
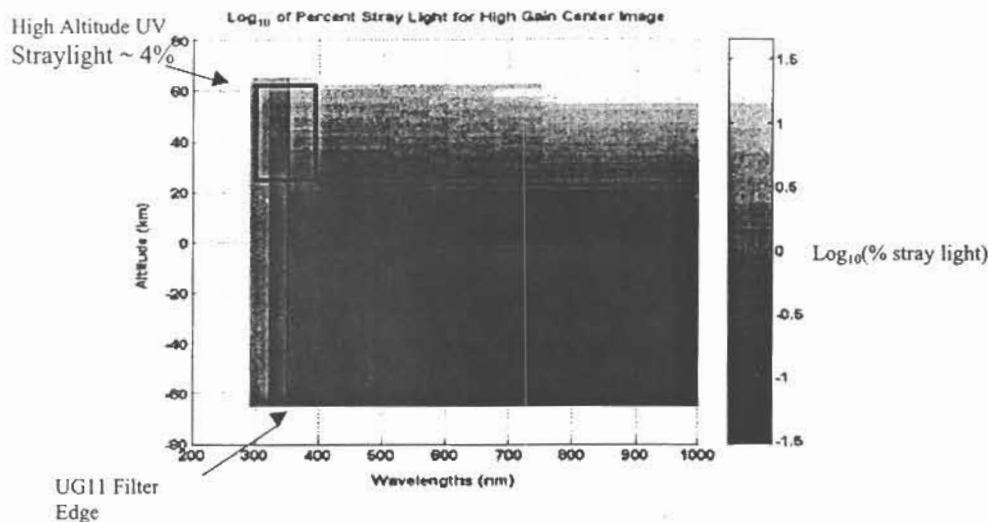
Figure 13    Limb Stray Light Map shows stray light at altitudes and wavelengths of concern to be <4% in the UV and <10% in the IR.

## 6.  CCD FOCAL PLANE

The optical detector used in both Nadir spectrometers is a custom split frame transfer Charge-Coupled Device (CCD)-based device manufactured specifically for the OMPS program by Marconi Applied Technologies. The CCD is a 340 (column) x 740 (row) split frame transfer device operated in a backside illuminated configuration. The pixel pitch is 20 μm in the column (spectral) dimension and 25 μm in the row (spatial) dimension and every pixel in both the active and storage regions contains a lateral overflow antiblooming structure integrated into a 4-phase CCD architecture. A 3-phase serial clock CCD is used to read out each row of image data through an on-chip 2 stage, AC coupled source follower amplifier with integrated line clamp. During normal operation all 340 pixels in each row are read out of a single amplifier. A second redundant amplifier is located at the opposite end of each serial CCD and can be activated by applying power and reverse clocking the serial CCD. Each of the 2 serial outputs yield a 340 (pixel) x 390 (row) image at a rate of ~440k pixels per second. The charge capacity of the parallel and serial CCDs is 600k and 1200k electrons, respectively.

Temporal aggregation of images, using two integration periods and two optical gains, and pixel aggregation in the spectral dimension are performed off-chip. To maintain sufficiently low dark current and charge transfer inefficiency through end of life, the CCD used in the Limb spectrometer is actively cooled. The CCD in the Limb spectrometer is oriented such that the spectral information varies with row position and spatial information with pixel position.

Each CCD is housed in a custom evacuated focal plane assembly that includes a thermo electric cooler (TEC), two temperature sensors, hermetically sealed electrical contacts, a contamination getter, a window, and a window heater (see Figure 9). The heater is used to keep the window above the instrument temperature. Electrical contacts to the CCD, temperature sensors and TEC are made through brazed side-wall connectors that terminate on an electronics PCB (termed the Pre-Amp board) that surrounds the focal plane assembly. All clock drivers, DC biases, and output pre-amplifiers are co-located on the Pre-Amp board to minimize the noise of the FPA.
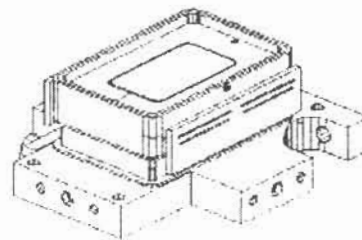


Figure 14    Diagram of the focal plane assembly

## 7. CALIBRATION

On-orbit calibration is planned for measurement of pixel gain, linearity, dark current, and wavelength. Since the limb sensor's measurements are used to determine the ratio of radiances between different altitudes it is important that any change in pixel gain be known. The pixel gain is determined by rotating a solar illuminated diffuser in front of the sensor field-of-view.

Two diffusers, a working diffuser and a reference diffuser, are used to reduce the effects of long-term degradation, due principally to contamination. The transmissive diffusers are attached to the solar calibration wheel (see Figure 1) and are composed of a microlens array and two rough diffuse surfaces on fused silica. This approach reduces goniometric errors to <0.25% and provides for a smaller package than that provided by reflective diffusers. Prelaunch goniometric calibration of the diffusers will characterize their scattering properties as a function of the incidence angles for which solar measurements are anticipated in orbit. During the 148 seconds available for solar calibration the working diffuser pair is moved sequentially in front of the three pairs of apertures, providing pixel signals which have an SNR of >500 for wavelengths less than 400 nm and >1250 for all other wavelengths. To satisfy the long-term stability requirement of ≤2% change over 7 years on orbit, the working diffuser is used weekly and the reference diffuser is used once every six months, thus limiting the effects of contamination. Whenever a diffuser is not in use it is protected from exposure to UV radiation and contamination by the calibration housing. Wavelength calibration is also performed during the solar calibration by making use of the spectral structure of the solar Fraunhofer lines.

Changes in both the CCD pixel dark current and the signal linearity of the on-chip output amplifier will result from exposure to radiation. Both of these performance parameters are measured once a week with the calibration/door rotor in the closed position during the dark part of the orbit. The measurement of CCD linearity relies on a stable LED light source and reproducible and accurate shutter timing obtained by changing the integration time of the CCD. The total linearity measurement takes approximately 60 seconds and will provide linearity knowledge to within approximately 0.2%.

## 8. ELECTRONICS

The main electronics box (MEB) handles power switching and distribution, instrument control, data conversion, mechanism interface and calibration control. All printed wiring assemblies use a VME 6U x220 form factor printed wiring board. A second MEB (cold standby) is used for full redundancy. A programmable timing pattern generator is used to control CCD timing functions such as integration times, frame rates and pixel clock rates. In addition, hardware-based processing functions such as pixel co-adding and linearity correction are enabled via a command interface. The timing pattern generator may be controlled from the ground to allow for changes throughout the life of the instrument. The MEB receives analog data from the detector and converts it to 14 bit digital data. Digitized pixel data and telemetry data are sent to the processor board where they are reformatted and transmitted to the spacecraft via the 1553 bus.

The MEB power supply operates continuously but the Limb instrument supply is switched on as required. The MEB also controls the diffuser wheel mechanism, calibration LED's, detector TEC's and window heaters. The spacecraft selects which redundant MEB is operational and also selects one of four boot programs. The dimensions of the composite MEB are 28.82 cm long x 19.0 cm high x 9.73 cm wide with a weight of 11 kg. On orbit average power dissipation for the entire OMPS suite is approximately 45 watts.

## 9. CONCLUSION

A high-accuracy and high-reliability limb ozone profiling sensor has been designed by Ball Aerospace & Technologies Corp for NPOESS as part of the OMPS contract. The staring spectrometer architecture and hyperspectral coverage eliminate the need for any continuous-action mechanisms, increasing the reliability of the sensor. The modular design is compact and athermal, requiring only passive thermal control with the exception of the CCD. The engineering unit of this sensor will be built and tested in the fall and winter of 2001-2002. First flight is currently planned for 2008.

## REFERENCES

1. Graf, P. H., et al., The preliminary design of the Ozone Mapping and Profiler Suite (OMPS), *Proceedings of the Quadrennial Ozone Symposium*, pp. 757-758, Hokkaido University, Sapporo, 2000.
2. Bhartia, P. K., R. D. McPeters, C. L Mateer, L. E. Flynn, and C. Wellemeyer, Algorithm for the estimation of vertical ozone profiles from the backscattered ultraviolet technique, *J. Geophys. Res.*, *101*, 18,793-18,806, 1996.

3. Rusch, D. W., G. H. Mount, C. A. Barth, R. J. Thomas, and M. T. Callan, Solar Mesosphere Explorer ultraviolet spectrometer measurements of ozone in the 1.0-0.1 mbar region, *J. Geophys. Res., 89*, 11,677-11,687, 1984.

4. Aruga, T., and D. F. Heath, Determination of vertical ozone distributions by spacecraft measurements using a limb-scan technique, Appl. Opt., 21, 3047-3054, 1980.

5. Herman, B. M., D. E. Flittner, R. D. McPeters, and P. K. Bhartia, Monitoring atmospheric ozone from space limb scatter measurements, *Proc. SPIE, 2582,* 88-99, 1995.

6. McPeters, R. D., S. J. Janz, E. Hilsenrath, T. L. Brown, D. E. Flittner, and D. F. Heath, The retrieval of ozone profiles from limb scatter measurements: results from the Shuttle Ozone Limb Sounding Experiment, *Geophys. Res. Lett., 27,* 2597-2600, 2000.

7. Flittner, D. E., B. M. Herman, and P. K. Bhartia, Ozone profiles retrieved from limb scatter measurements: theory, *Geophys. Res. Lett., 27,* 2601-2604, 2000.

8. National Aeronautics and Space Administration, *Advanced Scanners and Imaging Systems for Earth Observations,* NASA SP-335, 1973.